Fuel 420 (2026) 138937

Contents lists available at ScienceDirect

Fuel

journal homepage: www.elsevier.com/locate/fuel

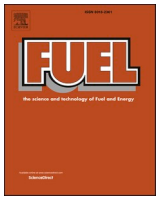

Full Length Article

Flow reactor oxidation study of oxymethylene ether (OME_{1-3}): Insights from molecular-beam mass spectrometry and kinetic modeling at elevated pressure☆

Thomas Bierkandt *, Trupti Kathrotia, Sascha Jacobs, Nina Gaiser, Jasmin Schmittner, Fabienne Werner, Joachim Schmid, Torsten Methling, Patrick Oßwald, Markus Köhler

Institute of Combustion Technology, German Aerospace Center (DLR), Stuttgart, Germany

ARTICLE INFO

Keywords:
OME
POMDME
MBMS
Flow reactor
Low-temperature oxidation
Kinetic modeling
NTC

ABSTRACT

This study investigates the oxidation of three oxymethylene ethers (OME_{1-3}) in a new elevated-pressure laminar plug-flow reactor, utilizing electron-ionization molecular-beam mass spectrometry. Experiments were conducted at an absolute pressure of 5 bar to mimic conditions more relevant to combustion systems but still allowing for the exploration of reaction kinetics and pathways in a controlled environment. The experimental work is supported by kinetic modeling using our in-house DLR Concise mechanism to gain deeper insights into OME_{1-3} combustion chemistry and highlight the controlling pathways. Kinetic modeling with two additional literature mechanisms was also employed to complement the findings. The measurements at constant carbon flow and similar conditions enable a systematic analogy among the three studied OMEs. The results reveal preferred formation of small C_1–C_2 hydrocarbons and oxygenates such as formaldehyde and methyl formate as combustion intermediates. Formation of methanol and formic acid was also observed during oxidation of all three OMEs, but the latter in significantly higher concentrations for both longer-chain OMEs. OME_1 shows only low reactivity in the low-temperature chemistry (LTC) regime, while the two larger OMEs have a higher reactivity in the LTC regime and also show a negative temperature coefficient behavior at the studied conditions. In line with previous reactor studies at atmospheric pressure, the reactivity of OME_2 and OME_3 is also similar at 5 bar, but is clearly distinguishable from OME_1. This work not only enhances our understanding of the fundamental chemistry underlying the oxidation mechanisms of OMEs, but also underscores their potential as cleaner fuel alternatives.

1. Introduction

Oxymethylene ethers (OMEs), also known as polyoxymethylene dimethyl ethers (POMDMEs), are especially emerging as promising alternative fuels for compression ignition engines that offer a sustainable and efficient solution to the challenges of conventional fossil diesel fuels [1]. Composed of carbon, hydrogen, and oxygen, OMEs can be synthesized from renewable resources, making them an environmentally friendly option [2]. Their unique chemical structure (CH_3O–$(CH_2O)_x$-CH_3) with no direct carbon–carbon bonds allow for lower emissions, especially in terms of particulate matter (PM) and nitrogen oxides (NO_x) [3], which are critical for reducing air pollution and combating climate change. OMEs can be blended with existing diesel fuels or used in advanced combustion engines, enhancing their versatility and integration into the current energy systems. Research into their properties and performance has shown that they can contribute to cleaner transportation and energy generation [1], aligning with global efforts to transition to more sustainable energy sources. As the demand for cleaner fuels grows, OMEs stand out as a viable candidate, paving the way for a sustainable society.

Understanding the combustion and oxidation mechanisms of OMEs is essential for optimizing fuel performance in various applications. Besides global combustion parameters, i.e., ignition delay times (IDTs) and flame speeds, especially detailed quantitative species measurements under controlled combustion environments are of crucial interest for development and validation of chemical kinetic mechanisms. In the last years, many studies have explored the formation of intermediates and the chemical kinetics involved in the low- and high-temperature

☆ This article is part of a special issue entitled: 'MCS13' published in Fuel.

* Corresponding author at: German Aerospace Center (DLR), Pfaffenwaldring 38-40, 70569 Stuttgart, Germany.
E-mail address: thomas.bierkandt@dlr.de (T. Bierkandt).

https://doi.org/10.1016/j.fuel.2026.138937
Received 29 October 2025; Received in revised form 16 February 2026; Accepted 25 February 2026
Available online 4 March 2026

oxidation processes of OMEs under ambient pressure, but species measurements for oxidation at elevated pressures are limited to some studies for OME_1 [4–10], also known as dimethoxymethane (DMM), and one study for OME_2 [10]. The experimental speciation study of dimethyl ether (DME), OME_1, and OME_2 by Lindner et al. was conducted for pyrolysis and oxidation (three equivalence ratios of 0.5, 1.0, and 2.0) between 975 and 1400 K in a single-pulse shock tube at 16 bar [10]. In our previous works, Gaiser et al. systematically studied the combustion of a series of OMEs up to OME_5 in atmospheric flow reactors [11,12] and in low-pressure flames [13] by electron-ionization molecular-beam mass spectrometry (EI-MBMS) and photoelectron photoion coincidence (PEPICO) spectroscopy. With these investigations, the isomers ethanol (C_2H_5OH) and dimethyl ether (CH_3OCH_3) were identified, separated, and quantified by PEPICO spectroscopy revealing its formation was underestimated by available chemical kinetic mechanisms. Pyrolysis and oxidation of OME_2 was intensely studied by De Ras et al. in flow reactors [14,15], rapid compression machine (RCM) [14], and in cool flames [16] with additional mechanism development and a special focus on the role of carbenes. Their flow reactor speciation measurements were conducted under pyrolytic conditions at elevated pressures of 3.4 bar [14] and 1.5 bar [15]. Recently, De Ras et al. also investigated the pyrolysis of larger OMEs (OME_{3-5}) theoretically and experimentally [17,18]. In the pyrolysis of OME_3, species measurements in tubular reactors at 1.5 bar (850–1150 K) and 3.4 bar (373–1073 K) have shown that OME_1, OME_2, and formaldehyde (CH_2O) are the main products of thermal decomposition at low temperatures, while H_2, CO, and CH_4 are dominant products at high temperatures [18]. Oxidation of $OME_{1–3}$ was studied in a jet-stirred reactor (JSR) by Wang et al. and their results showed that both OME_2 and OME_3 have a strong low-temperature oxidation reaction and a weak negative temperature coefficient (NTC) behavior [19]. Another JSR study of OME_{1-3} showed for pyrolysis at 1.03 atm and for temperatures between 450 and 1080 K that reactivity increases from OME_1 to OME_3 [20]. For OME_3 oxidation, quantitative species profiles were also measured at atmospheric pressure in a JSR by gas chromatography [21] and in a low-pressure laminar flame by photoionization molecular-beam mass spectrometry [22]. In a flow reactor oxidation study, it was experimentally shown and corroborated by chemical kinetic modeling that OME_3 (blended to toluene) leads to larger production of polycyclic aromatic hydrocarbons (PAHs) compared to neat toluene below 1050 K, but has an inhibiting effect on PAH formation at higher temperatures [23]. Very high-pressure conditions of up to 100 atm were studied for OME_1 in a JSR by Mei et al. showing that NTC behavior becomes weaker at 100 atm compared to 10 atm [4]. Marrodán et al. investigated the high-pressure oxidation of neat OME_1 [5] and OME_1/C_2H_2 mixtures [6] in a flow reactor at 20, 40, and 60 bar and found that OME_1 enhances the C_2H_2 reactivity under lean conditions [6]. For OME_1, Sun et al. have also studied its oxidation in a JSR at higher pressures of 10 atm and developed a kinetic model [7]. Under their investigated conditions, they have not observed noticeable low-temperature reactivity [7]. Concentration profiles in a JSR were also measured by Daly et al. for OME_1 oxidation at 5.07 bar with gas chromatography analysis and they postulated two surface-catalyzed reactions in OME_1 decomposition at temperatures below 800 K to yield formaldehyde + dimethyl ether ($OME_1 \rightarrow CH_2O + CH_3OCH_3$) and methanol + acetaldehyde ($OME_1 \rightarrow CH_3OH + CH_3CHO$) [8]. Vermeire et al. investigated the oxidation and pyrolysis of OME_1 at low to intermediate temperatures (500–1100 K) in a JSR and by kinetic modeling at near atmospheric pressure of 1.07 bar [24]. In a high-pressure shock-tube, species measurements were carried out by Herzler et al. for a CH_4/OME_1/air mixture with an equivalence ratio of 10 at 30 bar [9]. Peukert et al. also measured the temperature-dependent (1100–1430 K) composition of the stable reaction products from the thermal decomposition of OME_1 at 1.2–2.5 bar in a shock tube [25]. Additionally, they have determined high-temperature rate constants for overall decomposition of OME_1 [25].

Comprehensive chemical kinetic mechanisms, which include detailed low- and high-temperature chemistry of $OME_{1–3}$, were developed by Cai et al. [26], He et al. [27], Shrestha et al. [28], Wang et al. [19], Dinelli et al. [29], and Kathrotia et al. [30]. The mechanism of Cai et al. [26] was developed for $OME_{2–4}$ chemistry by an automatic reaction class-based mechanism generator with adopted reaction classes and rate rules from an OME_1 sub-mechanism of Jacobs et al. [31]. He et al. developed a mechanism for OME_3 in a systematic and hierarchical way based on ab initio/DFT studies on OME_1 and established rate rules from the literature [27]. The mechanism by Shrestha et al. [28] is constructed hierarchically and is based on their previous sub-mechanism of OME_1 [32] and the work of He et al. [27] for the additional sub-mechanisms of OME_2 and OME_3. The detailed $OME_{1–3}$ model of Wang et al. is developed based on a previous pyrolysis model [20] and monomolecular dissociation reaction of $OME_{1–3}$ and H-abstraction reaction by CH_3/H radicals [19]. Dinelli et al. developed a lumped mechanism for $OME_{2–5}$, which was constructed hierarchically with a novel methodology based on the coupling between the systematic construction of a semi-detailed mechanism employing reaction classes and rate rules, and a data-driven optimization for the refinement of the reaction rates of the different classes [29]. In the semi-detailed $OME_{0–5}$ mechanism of Kathrotia et al. [30], reaction rates of higher OMEs were determined from analogy of OME_1 and implemented in the previous published DLR Concise [33] for hydrocarbon combustion.

In this study, we have investigated the oxidation of OME_1, OME_2, and OME_3 at 5 bar in a new laminar plug-flow reactor by electron-ionization molecular-beam mass spectrometry between 473–1123 K to gain insights into their combustion chemistry at elevated pressures. The experimental results of OME_{1-3} were supported by kinetic modeling results from a recently published lumped OME mechanism of the CRECK Modeling Group [29], our own semi-detailed mechanism DLR Concise for OME low- and high-temperature chemistry [30] that was updated in this work, and additionally for the OME_1 measurements the mechanism of Jacobs et al. [31].

2. Methods

2.1. Experiment

Oxidation of OME_1 ($C_3H_8O_2$), OME_2 ($C_4H_{10}O_3$), and OME_3 ($C_5H_{12}O_4$) was studied in a new elevated-pressure plug-flow reactor at lean and rich conditions with equivalence ratios (Φ) of 0.8 and 1.2, respectively. OME_1 with a purity of 99% was purchased from Merck, while OME_2 and OME_3 were purchased from ASG Analytik with a purity of 98% each. The purity of OME_2 and OME_3 was checked with gas chromatography-mass spectrometry (GC–MS) before use and a purity of at least 98% was confirmed. For all investigated conditions, the same total carbon flow of 5 sccm was used and the reactor was operated at an absolute pressure of 5 bar. Measurements were carried out under a very high argon dilution (>99%) and for oven temperatures of 473 to 1123 K to cover low- and high-temperature oxidation. These temperatures correspond to residence times of 3.47 to 8.59 s in the heated oven zone of the reactor. Exact flow conditions are summarized in Table 1. The

Table 1
Inlet flow conditions and investigated temperature ranges for the performed oxidation studies of oxymethylene ethers.

Oxymethylene ether	OME_1		OME_2		OME_3	
Equivalence ratio	0.8	1.2	0.8	1.2	0.8	1.2
Fuel / sccm[a]	1.67		1.25		1.00	
O_2 / sccm[a]	8.34	5.55	7.81	5.21	7.50	5.00
Ar / sccm[a]	989.74		989.74		989.74	
C/O ratio	0.250	0.347	0.258	0.353	0.263	0.357
C/H ratio	0.375		0.400		0.417	
Pressure / bar	5		5		5	
Temperature / K	473–1123		473–1123		473–1123	

[a] sccm: standard cubic centimeters per minute at 1 atm and 273.15 K.

high dilution with the inert gas argon suppresses additional heat release from self-sustainable combustion. For comparable conditions to our previous OME oxidation flow reactor studies at atmospheric pressure [11,12,34], the same equivalence ratios of 0.8 and 1.2 were chosen, but the total carbon flow was reduced (5 sccm compared to 50 sccm in [11]) to account for the lower total flow in the new elevated-pressure flow reactor (1 slm compared to 10 slm).

To prevent catalytic wall reactions at high temperatures, the reactor consists of a quartz tube with an inner diameter of 8 mm and a length of 1500 mm, which is enclosed in a heat-resistant stainless-steel tube as a pressure shell and mounted in a split tube furnace (Carbolite Gero) with a heated length of 1040 mm. This furnace is also used in our actual atmospheric pressure setup [35]. A specially-designed expansion chamber connects the reactor to the EI-MBMS system and is operated at reduced pressure of 300 mbar. The pressure inside the reactor is automatically regulated by an expansion valve downstream. A sample behind this expansion valve at the end of the transfer line is withdrawn by a quartz nozzle and transferred into the ionization chamber of the reflectron time-of-flight mass spectrometer (RTOF-MS) through an additional two-stage expansion reducing the pressure to about $3 \bullet 10^{-5}$ mbar. This quenching process forms a molecular beam and preserves the actual gas composition at the time of sampling. The used EI-MBMS system allows determination of the exact elemental composition and species profiles of reactants, intermediates, and products are obtained as function of the oven temperature. The setup enables continuous temperature ramp measurements with one data point representing a temperature change of about 2.5 K. More information about the spectrometer system is given by Oßwald and Köhler [36]. A schematic of the new elevated-pressure plug-flow reactor system is presented in Fig. 1 together with a photo of the sampling nozzle, which protrudes into the transfer line. The new reactor was also used recently to study the oxidation of the two oxygenates ethyl *tert*-butyl ether (ETBE) and methyl *tert*-butyl ether (MBTE) at 5 bar [37].

All gases and the liquid fuels were metered by Coriolis mass flow controllers (Bronkhorst mini CORI-Flow) with high accuracy of ± 0.5% (gas) and ± 0.2% (liquid) of the actual flow rate. The oxymethylene ethers were vaporized at temperatures of 30°C (OME_1), 70°C (OME_2), and 120°C (OME_3) in a commercial vaporizer (Bronkhorst CEM W-101A) with argon as the carrier gas and mixed at the reactor inlet with oxygen. The fuel line and the reactor inlet and outlet, i.e., the parts of the reactor that are outside of the oven chamber, were heated up to 120°C to prevent any condensation.

The flow reactor was designed to approximate laminar plug flow with a flow rate of 1000 sccm at pressures and temperatures up to 20 bar and 1173 K, respectively. Fig. 2 shows according to Taylor [38] and Aris [39] the axial dispersion Pe_{ax}^{-1}, i.e., the reciprocal of the axial Péclet number, which is correlated with the molecular Péclet number Pe_m for five different temperatures. The calculated values are close to the minimum of the curve, which represents ideal plug-flow behavior, and are also comparable to other laminar plug-flow reactors operated at elevated pressures, e.g., Rasmussen et al. [40] or Hoener et al. [41].

The temperature profiles needed as input for kinetic modeling were measured by a thermocouple at four different oven temperatures (573, 773, 973, and 1173 K) with an argon flow of 1000 sccm. Individual temperature profiles for other oven temperatures were then calculated from a scaling law according to the procedure described by Oßwald and Köhler [36], whereby the measured profile at 773 K was used as the reference:

$$T(x)[\mathrm{K}] = \left(T_{\mathrm{ref}}(x) - T_0\right) \bullet \frac{1.005 \bullet T_{\mathrm{Oven}} - 4.0608\mathrm{K} - T_0}{T_{\mathrm{ref}}(850\mathrm{mm}) - T_0} + T_0 \quad (1)$$

In this equation, $T(x)$ is the gas temperature at a reactor position x for a given oven temperature T_{Oven}, $T_{\mathrm{ref}}(x)$ is the measured gas temperature at the reactor position x for an oven temperature of 773 K, T_0 is the inlet gas temperature, T_{ref}(850 mm) is the reference temperature measured for an oven temperature of 773 K at an reactor position of 850 mm within the isothermal oven zone, and the two constants are calculated from a temperature ramp measurement with the thermocouple placed at a reactor position of 850 mm to correct for thermal inertia of the system. Measured and scaled temperature profiles are presented in Fig. 2. The flow reactor has a long isothermal zone of about 800–900 mm length.

Quantitative mole fraction profiles of reactants, products, and combustion intermediates were determined for the oxidation of OME_1, OME_2, and OME_3 according to the procedure described in [36]. Uncertainties of the measured mole fractions depend on the individually used calibration method and are up to 20% for main species (obtained from the element balance, i.e., an internal calibration strategy) and up to 30% for directly calibrated intermediate species. For species which were quantified by the relative ionization cross section (RICS) method [42], the uncertainty is at least 50%, but can also increase up to a factor of 2–4 for labile species. The absolute uncertainty of the temperature, i.e., x-axis in the species mole fraction profiles, is ±20 K [36].

2.2. Modeling

Two recently published kinetic models were used for comparison to the measured elevated-pressure plug-flow reactor data sets of OME_1,

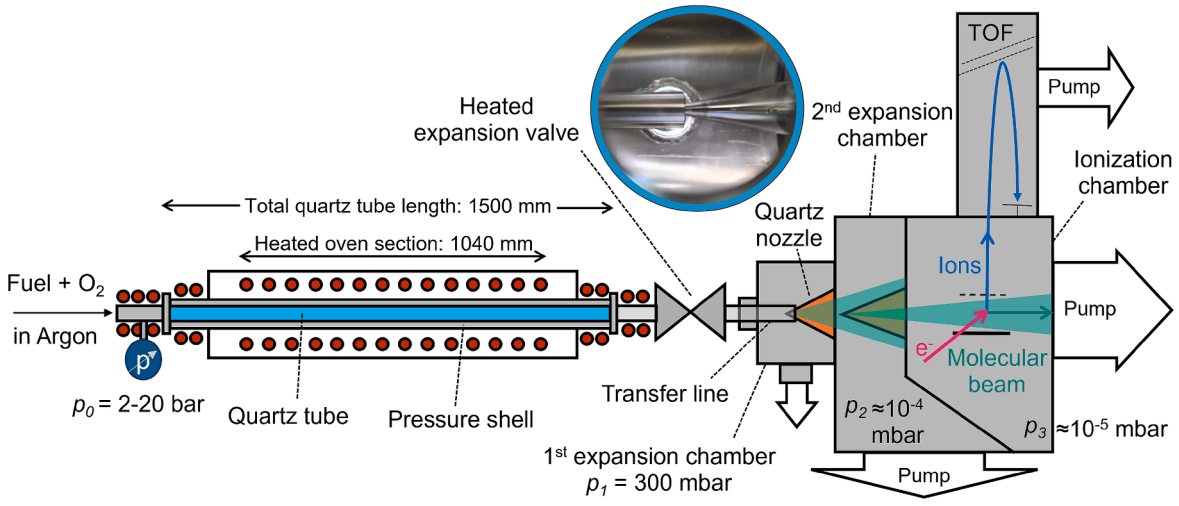

Fig. 1. Schematic of the new elevated-pressure plug-flow reactor coupled to a molecular-beam mass spectrometry system and a photo of the transfer line and the sampling nozzle.

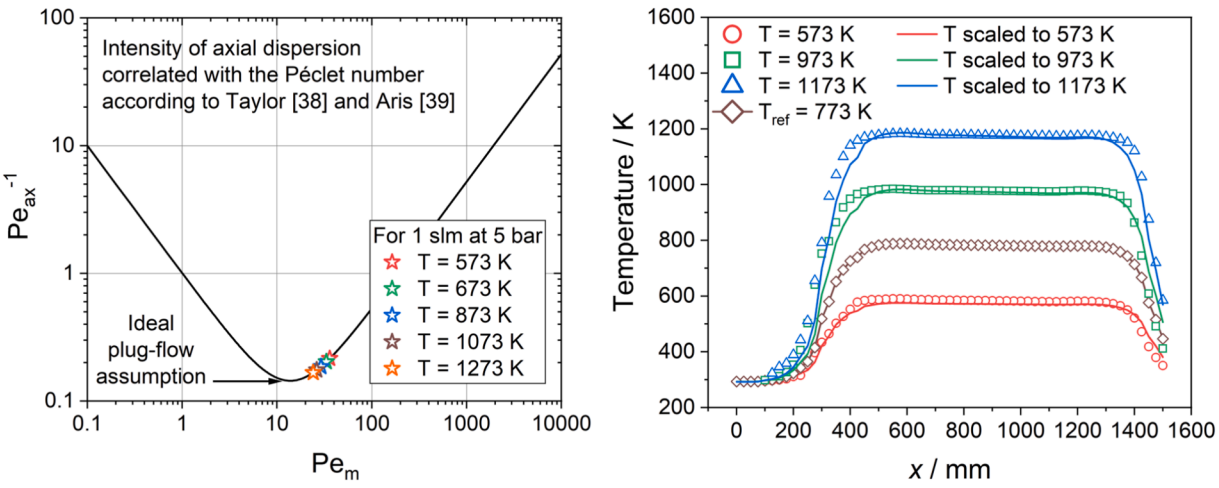

Fig. 2. Axial dispersion correlated with the molecular Péclet number (left) and temperature profiles of the new elevated-pressure plug-flow reactor (right).

OME_2, and OME_3. The first one is a compact, lumped mechanism with a C_0-C_3 core mechanism, literature sub-mechanisms for DME and OME_1, and sub-mechanisms of $OME_{2–5}$ developed by rate rules and optimization [29]. This mechanism from the CRECK modeling Group is hereafter named POLIMI. The second mechanism is our in-house DLR Concise, which is a semi-detailed mechanism for jet fuel surrogates [33] that was recently updated for oxygenated fuels including $OME_{0–5}$ [30]. Both mechanisms were extensively validated against IDTs, flame speeds, and species measurements. For OME_1, a third mechanism from the work of Jacobs et al. [31] was additionally used since its OME_1 sub-mechanism was also implemented into the POLIMI mechanism of Dinelli et al. [29]. Zero-dimensional plug-flow simulations were done for our measured conditions in both Cantera [43] and Chemical Workbench [44] by using the temperature profiles obtained from equation (Eq1) with temperature intervals of 10 K, and are cross-validated. The use of former is specifically to perform brute-force sensitivity analyses unavailable in the latter software. Temperature profiles are provided in the supplementary material together with the experimental mole fraction profiles.

In this work, few changes have been undertaken in DLR Concise [20] to reduce the sharp NTC behavior shown in model but not observed in the new experiments at elevated pressure of 5 bar. The most sensitive reaction found for such sharp NTC is the reaction (R1):

$$s\text{-}OME_x\text{-}OO \rightarrow OME_x\text{-}CY6 + OH \text{ (where x = 1–5)} \quad (R1)$$

$$OME_x\text{-}KET \rightarrow A + B + OH \text{ (where x = 2–5)} \quad (R2)$$

$$OME_x + HO_2 = p\text{-}OME_x{}^*\text{-}1 + H_2O_2 \text{ (where x = 2–5)} \quad (R3)$$

$$DME\text{-}1OO = 2\ COCO^* + O_2 \text{ (product updated)} \quad (R4)$$

$$OME_x = CO(CO)_yCO^* + OME_{(x\text{-}y\text{-}2)}{}^*\text{-}1 \quad (R5)$$

(x = 2–5; for each x, corresponding y = 0,1,…,x-2)

To further improve the prediction quality in the NTC range, the reactions (R2)–(R5) were also revised, albeit only capturing small effects. The resulting mechanism (hereafter referred to as the updated DLR Concise) is used in the present work for reaction pathways, sensitivity analyses, and the plug-flow simulations of the experiments. The reactions (R1)–(R5) along with their modified reaction rates are listed in Table S1 of the supplementary material.

3. Results and discussion

3.1. Main species and general fuel reactivity

To get a general overview on the different reactivities of the three studied OMEs, Fig. 3 shows the measured mole fraction profiles of the main species, i.e., the fuel (OME_1, OME_2, or OME_3), oxygen (O_2), carbon monoxide (CO), carbon dioxide (CO_2), hydrogen (H_2), and water (H_2O), for the lean condition with equivalence ratio of 0.8. This figure also shows comparisons between the experimental results and the modeling results of the mechanisms POLIMI [29], Jacobs [31] (only for OME_1), and DLR Concise (original [30] and updated model). The shaded areas represent the experimental uncertainties of 20% for main species. Mole fraction profiles of the main species for the rich condition with equivalence ratio of 1.2 are presented in Fig. S1 in the supplementary material. Unless otherwise stated, the following discussion refers to the lean condition.

Since the flow rates were adjusted to have the same amount of carbon in the system under all studied conditions, the inlet mole fractions of the three fuels are obviously different and the C/H ratios also differ. As seen in Table 1, they increase from OME_1 to OME_3. Under the same studied equivalence ratio, the C/O ratios show the same trend (see also Table 1). OME_1 starts to decompose very slowly at about 550 K and more rapidly above 800 K, where also O_2 consumption starts (see Fig. 3). The fuel OME_1 is then totally consumed above 850 K. The POLIMI model captures the decomposition of OME_1 quite well, but does not reproduce the low-temperature reactivity below 800 K (clearly visible in intermediate species profiles of oxygenates discussed below in section 3.2). In contrast, the DLR Concise shows significant reactivity below 800 K, leading to an NTC behavior that is neither observed in the experiment nor in the predictions of the POLIMI. The OME_1 sub-mechanism, including the pressure-dependent reactions of the POLIMI model [29], was adopted from the work of Jacobs et al. [31], as described in [45], and is not accounted for in the low-temperature chemistry of DLR Concise. This may explain the stronger pronounced OME_1 decomposition in the DLR Concise simulation. The Jacobs mechanism also shows no NTC behavior and best predicts the initial OME_1 conversion at around 650 K, but is slightly faster than the POLIMI model above 750 K. In general, the differences between the two models are small and could be attributed to the different C_0–C_1 base chemistry. Sun et al. have studied the oxidation of OME_1 at 10 atm in a jet-stirred reactor and have also not observed obvious low-temperature chemistry [7]. However, their data is quite well reproduced by the DLR Concise model [30].

In comparison to OME_1, OME_2 and OME_3 show higher reactivity and already start to decompose at 550–560 K. Both of them show high

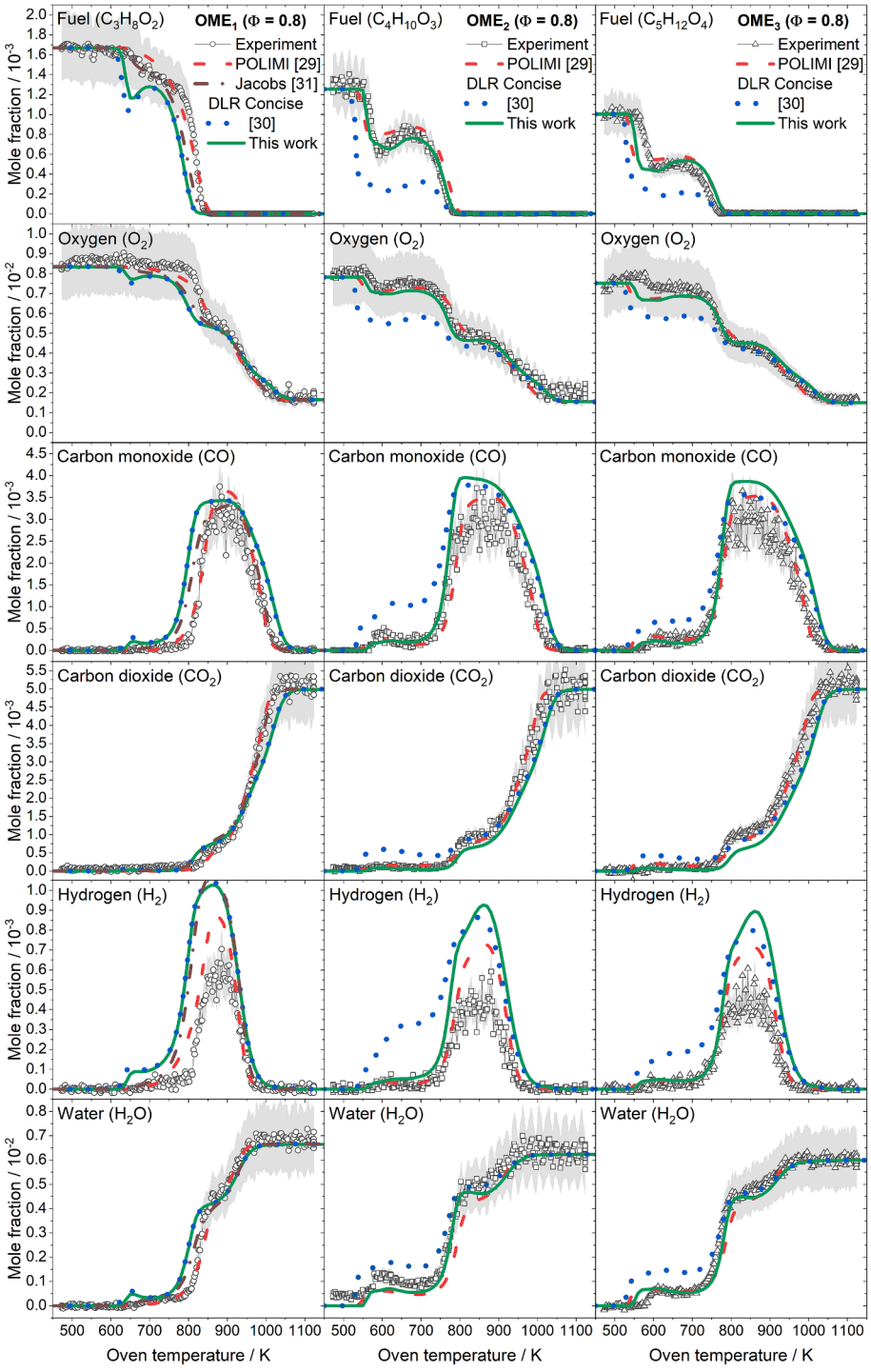

Fig. 3. Experimental (symbols) and simulated (lines) mole fraction profiles of major species (fuel, O_2, CO, CO_2, H_2, H_2O) for lean oxidation (Φ = 0.8) of OME_1 (left), OME_2 (center), and OME_3 (right). Shaded areas are the experimental uncertainties of the mole fraction (y-axis), while absolute uncertainty of the temperature (x-axis) is ±20 K in the experiment.

reactivity especially in the low-temperature chemistry (LTC) regime and an NTC behavior between 595–670 K (OME_2) and 610–690 K (OME_3), respectively. However, if the uncertainties of 20% in the fuel mole fractions and ±20 K in the oven temperatures are taken into account, OME_2 and OME_3 have a similar reactivity. This is consistent with our previous detailed analysis performed at atmospheric conditions in a flow reactor and also in different combustion setups [30], according to which the reactivity of OME_0 and OME_1 are distinguishable from higher OMEs but no distinction is seen for $OME_{2\text{-}5}$. The NTC is also predicted by the POLIMI model, but is weaker pronounced than in the experiments. For OME_3 simulations, the fuel decomposition is slightly shifted to smaller temperatures.

In the predictions of the original DLR Concise, the low-temperature oxidation process of OME_2 and OME_3 are too much pronounced, which was found due to the selected reaction rate of reaction (R1). Due to their weak rate, the accelerating low-temperature branch competes with decelerating providing stronger NTC behavior. That is, the rate of reaction (R1) influences the branching between cyclic ethers and

ketones from OME_x-QOOH radical decomposition. We updated the rate of this reaction including few small changes as listed before (see section 2.2). The result is a preferential formation of cyclic ethers, which inhibits the global reactivity [30] and lead to less pronounced LTC. With these changes, the experimental profiles of the fuels OME_2 and OME_3 are well reproduced by the updated model whereas mole fractions of OME_1 are within the experimental uncertainties. The effect is stronger pronounced for OME_2 and OME_3 compared to OME_1 and has also a particularly large impact on formation of intermediates at low temperatures (see section 3.2).

At lean conditions, CO and H_2 are intermediates which are fully oxidized to CO_2 and H_2O at the reactor outlet for higher oven temperatures. For the other studied equivalence ratio, incomplete combustion is observed (see Fig. S1) and CO and H_2 are also detected at the highest oven temperature of 1123 K. All models can predict within the measurement uncertainty the product composition at these highest oven temperatures. Note that the different yields of H_2O reflect the different C/O and C/H ratios of the three OMEs as mentioned before (see Table 1).

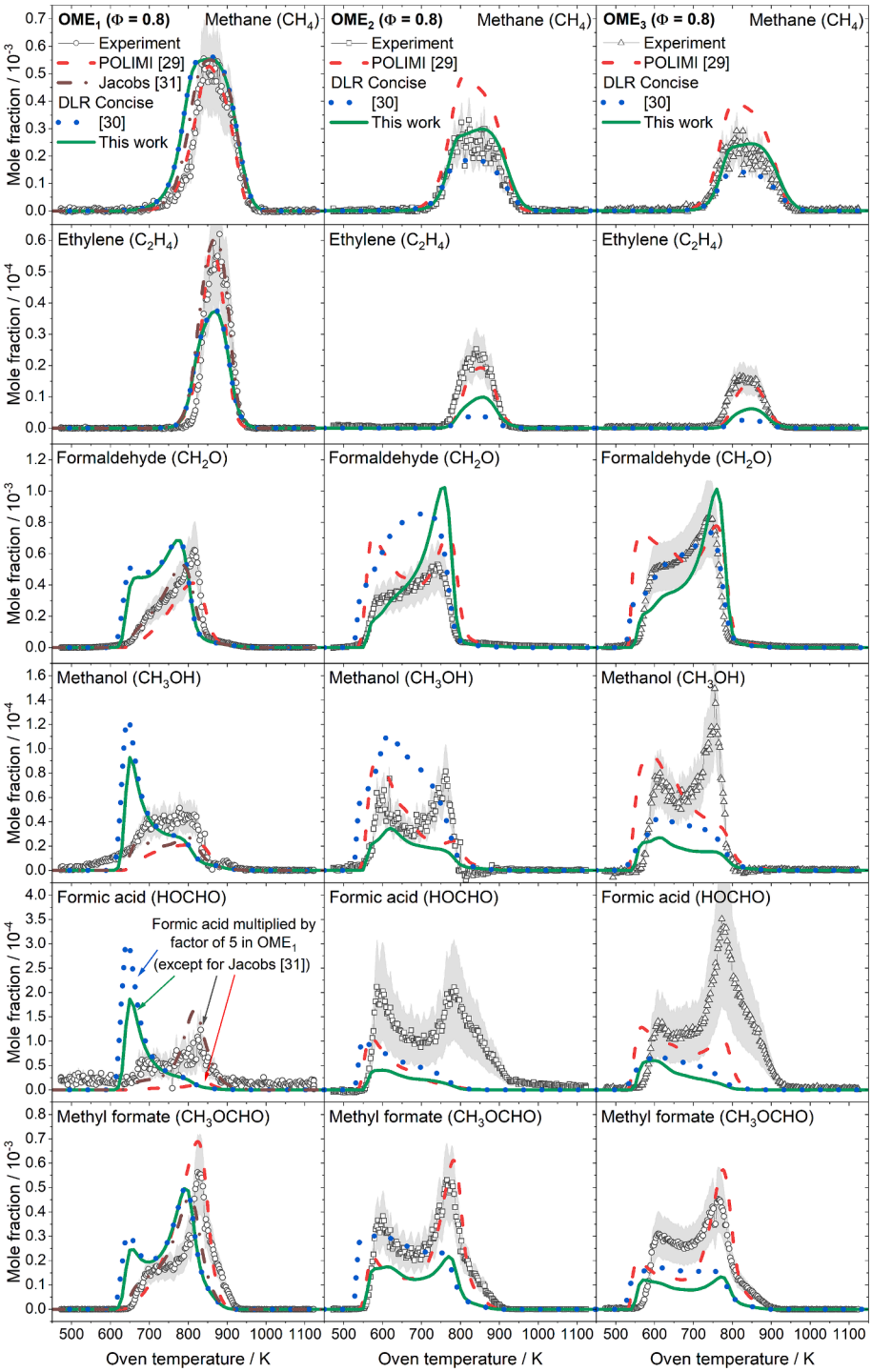

Fig. 4. Experimental (symbols) and simulated (lines) mole fraction profiles of intermediate species (CH_4, C_2H_4, CH_2O, CH_3OH, HOCHO, CH_3OCHO) for lean oxidation ($\Phi = 0.8$) of OME_1 (left), OME_2 (center), and OME_3 (right). Shaded areas are the experimental uncertainties of the mole fraction (y-axis), while absolute uncertainty of the temperature (x-axis) is ±20 K in the experiment.

3.2. Intermediate species and reaction path analysis

To further discuss the decomposition steps of OMEs, a deeper look into the formed species pool during their oxidation is necessary. Therefore, Fig. 4 shows the mole fraction profiles of the two small hydrocarbons methane (CH_4) and ethylene (C_2H_4) and the four oxygenates formaldehyde (CH_2O), methanol (CH_3OH), formic acid (HOCHO), and methyl formate (CH_3OCHO). These species were detected under our investigated conditions in highest mole fractions on the order of 10^{-5}–10^{-3} (10–1000 ppm). Formation of ethane (C_2H_6) and C_2H_6O was also observed (see mole fraction profiles in the supplementary material). Compared to hydrocarbons with equivalent carbon number, the overall detectable species pool is generally small for OME combustion. With the exception of formic acid, all other intermediate species presented in Fig. 4 were directly calibrated. The calibration factor of formic acid was determined by the RICS method with ethanol as the reference species as was also done in previous work [11]. The displayed measurement uncertainties are at least 50% for formic acid and 30% for all other intermediates presented in Fig. 4. For the other studied equivalence ratio of 1.2, the intermediate species mole fraction profiles are presented in Fig. S2 of the supplementary material.

3.2.1. Insights into OME_1 reaction chemistry

For OME_1, the POLIMI and the Jacobs model can reproduce the general profile shape and also the absolute quantities of the detected intermediates quite well as seen in Fig. 4. There are only larger discrepancies for methanol and formic acid. The latter is mainly formed from formaldehyde via reactions (R6) and (R7) and the observed differences, i.e., the underprediction by the POLIMI and the overprediction by the Jacobs model, can be attributed to large differences in the rate of reaction (R6). The DLR Concise model overpredicts the reactivity in the LTC regime but can also satisfactorily predict the profiles at the higher temperatures. Slightly above 550 K, the methanol signal starts increasing in the experiment under lean conditions which is not covered by the models. Principally, methanol can be formed early from reaction channels where the methoxy radical is involved according to reactions (R8) and (R9), where OME_1-R is the primary or secondary fuel radical. It is conceivable that methanol is directly formed from unimolecular decomposition of OME_1 according to the roaming reaction (R10), which plays an important role in OME_1 chemistry. Yu et al. have shown that this reaction is initiated by H migration to yield methanol and methoxymethylene (CH_3OCH), which can further dissociate at small excess energies to CH_3 and HCO radicals [46].

$$CH_2O + OH = HOCH_2O \quad (R6)$$

$$HOCH_2O = HOCHO + H \quad (R7)$$

$$HO_2 + CH_3O = O_2 + CH_3OH \quad (R8)$$

$$CH_3OCH_2OCH_3\ (OME_1) + CH_3O = OME_1\text{-}R + CH_3OH \quad (R9)$$

$$CH_3OCH_2OCH_3\ (OME_1) \rightarrow CH_3OH + CH_3 + HCO \quad (R10)$$

Nevertheless, more important stable combustion intermediates in OME_1 oxidation besides methanol are formaldehyde (CH_2O) and methyl formate (CH_3OCHO) as seen from the reaction path analysis in Fig. 5 obtained with the updated DLR Concise mechanism. It shows the main carbon flow under the investigated lean conditions for a temperature of 700 K (about 25% fuel conversion where the updated DLR Concise mechanism still shows an NTC behavior) and a reactor length of 1300 mm (end of the isothermal section of the flow reactor). OME_1 decomposition is majorly initiated by H-abstraction reaction with OH radicals to yield equally primary (OME1*-1) and secondary fuel radicals (OME1*-3), while minor unimolecular decomposition of OME_1 is over (R10). This is apparent because, at such low temperatures, thermal decomposition is not expected to be dominant.

Both fuel radicals contribute to formation of formaldehyde showing its importance in OME oxidation. The primary fuel radical directly decomposes by β-scission to CH_2O and the dimethyl ether radical (R11), which is also a direct source of formaldehyde over reactions (R12) and (R13) or through low-temperature oxidation pathways over the methoxymethyl-peroxy radical (DME*-1OO). The secondary fuel radical decomposes by β-scission reaction to yield methyl formate and methyl radicals (R14):

$$CH_2OCH_2OCH_3\ (OME1\text{*-}1) = CH_2OCH_3\ (DME\text{*-}1) + CH_2O \quad (R11)$$

$$CH_2OCH_3\ (DME\text{*-}1) = CH_3 + CH_2O \quad (R12)$$

$$CH_2OCH_3\ (DME\text{*-}1) + O_2 \rightarrow OH + 2\ CH_2O \quad (R13)$$

$$CH_3OCHOCH_3\ (OME1\text{*-}3) \rightarrow CH_3OCHO + CH_3 \quad (R14)$$

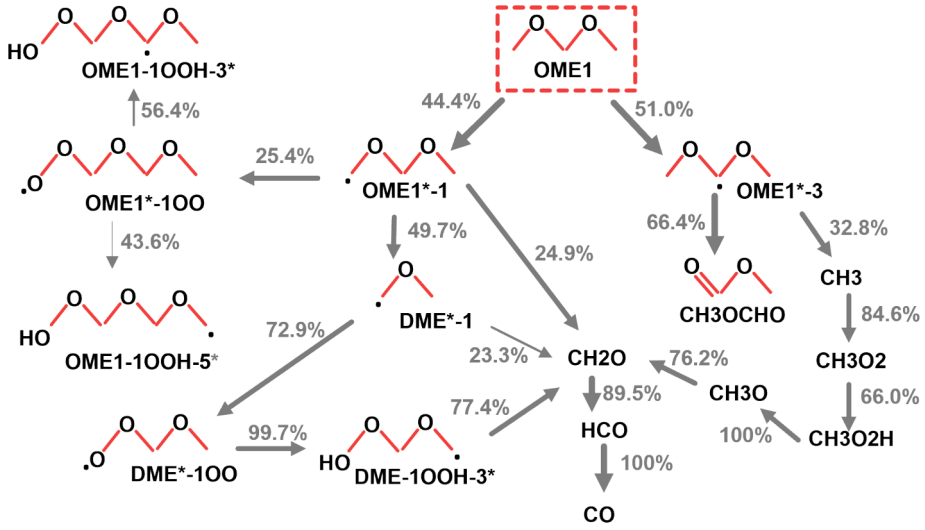

Fig. 5. Reaction path analysis at 700 K (25% fuel conversion) and a reactor length of 1300 mm for lean oxidation ($\Phi = 0.8$) of OME_1 obtained with the updated DLR Concise mechanism. Thickness of arrows represent the carbon flux and indicate the main consumption pathways. Percentages next to arrows give the contribution of individual decomposition rates of a species. Only carbon fluxes higher than 10% are shown.

3.2.2. Larger oxymethylene ethers: OME_2 and OME_3

For the two larger OMEs, signals of all oxygenated species displayed in Fig. 4 rises steeply at temperatures of 550–570 K due to the observed low-temperature oxidation. Compared to the DLR Concise model, the POLIMI model shows distinct peak around 550 K in formaldehyde profiles of OME_2 and OME_3 which are not seen in the measurements. The reaction pathways for OME_2 and OME_3 are shown in Fig. 6 and Fig. S3 for a temperature of 700 K corresponding to a fuel conversion of about 40 and 50%, respectively. While the formation of the secondary fuel radical was slightly favored in OME_1 oxidation, there is a change in the dominant reaction pathways for the formation of the primary fuel radical in OME_2 and OME_3. In contrast to alkanes, the formation of primary radicals in OME combustion is generally more dominant compared to secondary radicals due to the weak C-O bond. Additionally, the low-temperature chemistry at the secondary position is successfully completed by low energy barrier of reaction forming formic acid esters such as methyl formate in OME_2 [30].

Methyl formate is a key intermediate species in OME oxidation and is directly formed from the secondary fuel radicals as β-decomposition product under lower and higher reaction temperatures. This formation pathway explains the high concentrations of methyl formate above 750 K. In the low-temperature regime, methyl formate is also a branching product from QOOH-type radicals. The prediction of methyl formate is slightly better with the POLIMI model for the high-temperature route (second peak in the mole fraction profile of methyl formate), where the modeling results well reproduce both the measured mole fraction and the peak position.

With OME_2 and OME_3 as the fuel, we were also able to detect the methyl hydroperoxide (CH_3O_2H), a branching agent formed from hydrogen abstraction on the fuel by methyl peroxy radicals (CH_3O_2) or from reaction of hydroperoxyl radicals (HO_2) with CH_3O_2:

$$CH_3O(CH_2O)_2CH_3\ (OME_2) + CH_3O_2 = OME_2\text{-}R + CH_3O_2H \quad (R15)$$

$$CH_3O(CH_2O)_3CH_3\ (OME_3) + CH_3O_2 = OME_3\text{-}R + CH_3O_2H \quad (R16)$$

$$HO_2 + CH_3O_2 = CH_3O_2H + O_2 \quad (R17)$$

Methyl hydroperoxide peaks at 580–590 K with maximum mole fractions of $1.4\bullet10^{-5}$ and $6.1\bullet10^{-6}$ during lean oxidation of OME_2 and OME_3, respectively (see mole fraction profiles in the supplementary material). This elusive species decomposes when the temperature rises mainly to hydroxyl (OH) and methoxy (CH_3O) radicals (R18), where the methoxy radical is then a source of H radicals (R19):

$$CH_3O_2H = OH + CH_3O \quad (R18)$$

$$CH_3O(+M) = CH_2O + H(+M) \quad (R19)$$

Mole fraction of formic acid is significantly higher in OME_2 und OME_3 oxidation compared to OME_1 (more than a factor of 10 in the experiment). It can be formed via formaldehyde according to reactions (R6) and (R7). Especially at increasing temperatures, formation of formic acid is noticeably underpredicted by both models (POLIMI and DLR Concise) and more investigations are necessary to identify potential missing formation pathways not included in the mechanisms.

At higher temperatures, hydrocarbon species are also detected, but not larger than C_2 even under rich conditions. Ethane is typically built-up on methyl radical recombination reaction. Peak positions of methane and ethylene are predicted by both models very well, but the absolute mole fraction of C_2H_4 is still underestimated by the updated DLR Concise model for the larger OMEs. Since ethylene is a decomposition product of ethane, this species is also underestimated by the DLR Concise model (not shown here). Overall, the POLIMI model predicts better the measured elevated-pressure OME species profiles, but is also not fully able to capture all species profiles. One potential factor contributing on the better performance of the POLIMI model might be the included pressure-dependent rate constants for the low-temperature oxidation of OME_1 from the work of Jacobs et al. [31]. Nevertheless, both the POLIMI and the updated DLR Concise mechanisms can predict the key species in OME oxidation satisfactorily for the investigated conditions at elevated pressure of 5 bar.

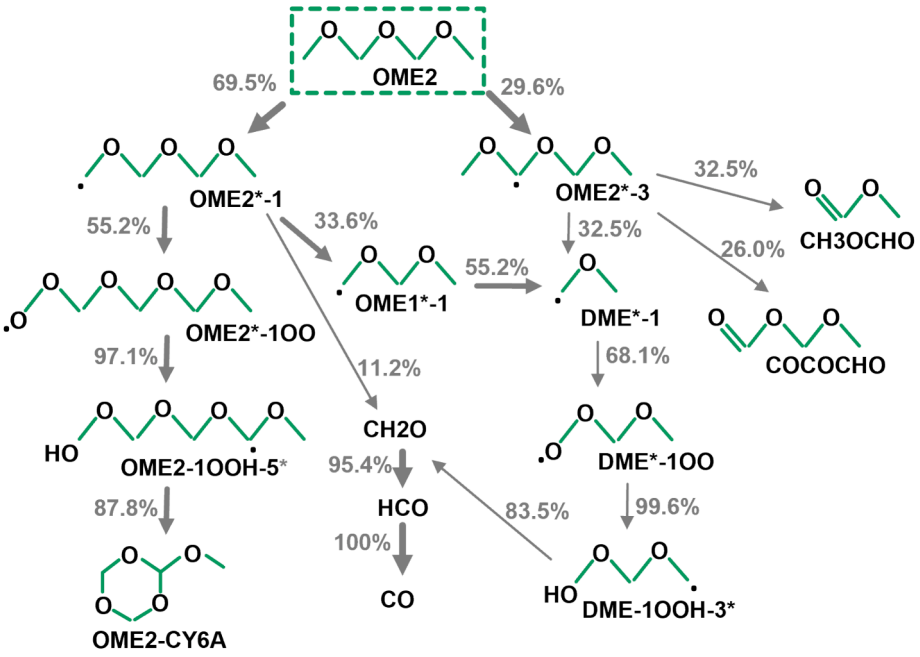

Fig. 6. Reaction path analysis at 700 K (40% fuel conversion) and a reactor length of 1300 mm for lean oxidation ($\Phi = 0.8$) of OME_2 obtained with the updated DLR Concise mechanism. Thickness of arrows represent the carbon flux and indicate the main consumption pathways. Percentages next to arrows give the contribution of individual decomposition rates of a species. Only carbon fluxes higher than 10% are shown.

3.3. Sensitivity analysis

Reactions sensitive to fuel conversion of all three OMEs are shown in Fig. 7 for flow reactor conditions similar to those in the reaction pathway analyses (Fig. 5, Fig. 6, and Fig. S3). The brute-force sensitivity (σ) with the updated DLR Concise mechanism is carried out where we investigate shift of first local maximum (max1) for each fuel ($OME_{1–3}$) around 700 K in the flow reactor. Here, positive sensitivity represents decrease in fuel consumption thereby slowing reactivity and negative sensitivity represents increased fuel consumption thereby accelerating effects on global reactivity.

At moderate temperatures and high pressures, stabilization of H and O_2 to form hydroperoxyl (HO_2) via reaction $H + O_2 \rightarrow HO_2$ is favored to chain branching. Thus, the role of the peroxy radical is apparent, where the reaction forming and consuming HO_2 radicals, and is sensitive to all three fuels studied. At around 700 K (in the NTC regime), the reactions leading to primary radicals from OMEs (Fig. 5, Fig. 6, and Fig. S3) are most sensitive to the temperature change. The H-abstraction of fuel to primary radical (with OH and HO_2) are responsible for the increased reactivity which are shown in Fig. 7 with negative sensitivity.

At lower temperatures and NTC conditions, all OMEs produce DME*-1 (CH_3OCH_2) from primary fuel radicals (*p*-OMEx-1) involved in the process (Fig. 5, Fig. 6, and Fig. S3). The DME*-1 then reacts with O_2 forming DME*-1OO in accelerating branch leading to OH radicals. Thus, this reaction shows negative sensitivity for all OMEs. Whereas, the *β*-scission of the QOOH radical forming one hydroxyl radical and two formaldehyde molecules (DME*-1OOH-3* → 2 CH_2O + OH), or cyclic ethers (OMEx-1OOH-5* → OMEx-CY6A + OH) is a degenerate branch showing positive sensitivity. The former competes with accelerating reaction DME*-1OOH-3* + O_2 or with CH_2O + OH → HCO + H_2O consuming formaldehyde. The reactions consuming secondary fuel radical (OMEx*-3) via *β*-scission shows opposite sensitivity forming either methyl radical or methyl formate. At intermediate temperatures, the methyl radical reacts to form a methyl peroxy radical ($CH_3 + O_2 + M$ → CH_3O_2 + M), which is a major sink for CH_3 and is a degenerate channel giving positive sensitivity. The formation of methyl formate from secondary radical has very low energy barrier and persists even at low temperatures giving increased reactivity.

A sensitivity analysis was also carried out with the POLIMI mechanism under comparable conditions, i.e., at around 700 K, and is presented in Fig. S4 of the supplementary material. Since this mechanism shows no NTC behavior for OME_1, the sensitivity analysis was only performed for the two larger OMEs (OME_2 and OME_3). With the POLIMI mechanism, the H-abstraction reaction of the fuel with OH forms fuel radicals and H_2O. This reaction shows the highest negative sensitivity and promotes reactivity, while the reaction that consumes CH_2O and OH shows the highest positive sensitivity and inhibits reactivity.

4. Conclusions

The presented study provides valuable insights into the oxidation chemistry of three oxymethylene ethers ($OME_{1–3}$) under elevated-pressure conditions, using a novel plug-flow reactor operated at 5 bar and temperatures between 473 and 1023 K to cover low- and high-temperature oxidation pathways for lean and rich conditions. Through a combination of electron-ionization molecular-beam mass spectrometry measurements and kinetic modeling with three chemical kinetic mechanisms, we successfully identified key combustion intermediates such as formaldehyde (CH_2O) and methyl formate (CH_3OCHO) and elucidated their roles in the oxidation pathways of OMEs. Generally, the species pool is relatively small compared to hydrocarbon oxidations and very similar for all investigated OMEs. Only C_1-C_2 hydrocarbons (methane, acetylene, ethylene, and ethane) were detected, which shows the great soot reduction potential of OMEs. Quantitative species profiles for oxidation of OME_2 and OME_3 were measured for the first time, to the best of our knowledge, in a flow reactor at elevated pressure. Overall, 15–20 mole fraction profiles of combustion species for each of the studied OMEs are provided. The results show that OME_1 has only a low reactivity in the low-temperature chemistry regime and no NTC behavior, while both OME_2 and OME_3 have a higher reactivity in the LTC regime and additionally show an NTC behavior. As in our previous work [30], the larger OMEs show comparable reactivity, which is, however, clearly distinguishable from OME_1. Our in-house mechanism DLR Concise [30] was slightly updated to better predict the newly measured species mole fraction profiles at elevated pressure in agreement with two other literature mechanisms, which were used without any modification. The combination of EI-MBMS and kinetic modeling contributes to a better understanding of OME combustion chemistry at elevated pressures and lays the groundwork for future studies aimed at optimizing the use of OMEs in practical combustion applications, such as

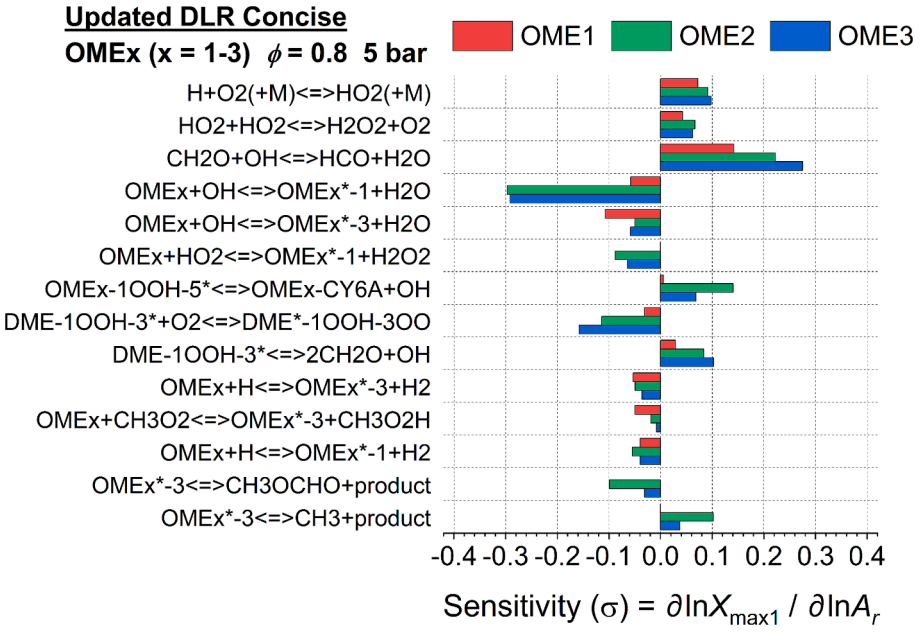

Fig. 7. Brute-force reaction sensitivity analysis for lean oxidation (Φ = 0.8) of $OME_{1–3}$ obtained with the updated DLR Concise mechanism.

in advanced internal combustion engines.

CRediT authorship contribution statement

Thomas Bierkandt: Writing – original draft, Visualization, Validation, Methodology, Investigation, Formal analysis, Conceptualization. **Trupti Kathrotia:** Writing – original draft, Methodology. **Sascha Jacobs:** Writing – review & editing, Methodology. **Nina Gaiser:** Writing – review & editing, Investigation. **Jasmin Schmittner:** Writing – review & editing, Investigation. **Fabienne Werner:** Writing – review & editing, Investigation. **Joachim Schmid:** Investigation. **Torsten Methling:** Writing – review & editing, Funding acquisition. **Patrick Oßwald:** Writing – review & editing, Supervision. **Markus Köhler:** Writing – review & editing, Supervision, Funding acquisition.

Declaration of competing interest

The authors declare that they have no known competing financial interests or personal relationships that could have appeared to influence the work reported in this paper.

Acknowledgments

We acknowledge financial support from the DLR project NeoFuels and thank Norbert Ackermann for the purity determination of OME_2 and OME_3 by GC-MS.

Appendix A. Supplementary data

Supplementary data to this article can be found online at https://doi.org/10.1016/j.fuel.2026.138937.

Data availability

Supporting figures, updated reaction rates in DLR Concise, experimental mole fraction profiles, and the temperature profiles are included in the supplementary material.

References

[1] Pitsch H, Goeb D, Cai L, Willems W. Potential of oxymethylene ethers as renewable diesel substitute. Prog Energy Combust Sci 2024;104:101173.
[2] Geitner R, Schuett T, Zechel S, Schubert US. Advancements and challenges in the synthesis of oxymethylene ethers (OMEs) as sustainable transportation fuels. Chem Eur J 2024;30:e202401570.
[3] Omari A, Heuser B, Pischinger S, Rüdinger C. Potential of long-chain oxymethylene ether and oxymethylene ether-diesel blends for ultra-low emission engines. Appl Energy 2019;239:1242–9.
[4] Mei B, Wang Z, Thawko A, Liu N, Thompson L, Attinger J, et al. Dimethoxymethane low- and intermediate-temperature oxidation up to 100 atm. Proc Combust Inst 2024;40:105650.
[5] Marrodán L, Royo E, Millera Á, Bilbao R, Alzueta MU. High pressure oxidation of dimethoxymethane. Energy Fuels 2015;29:3507–17.
[6] Marrodán L, Millera Á, Bilbao R, Alzueta MU. Experimental and modeling evaluation of dimethoxymethane as an additive for high-pressure acetylene oxidation. Chem A Eur J 2022;126:6253–63.
[7] Sun W, Tao T, Lailliau M, Hansen N, Yang B, Dagaut P. Exploration of the oxidation chemistry of dimethoxymethane: Jet-stirred reactor experiments and kinetic modeling. Combust Flame 2018;193:491–501.
[8] Daly CA, Simmie JM, Dagaut P, Cathonnet M. Oxidation of dimethoxymethane in a jet-stirred reactor. Combust Flame 2001;125:1106–17.
[9] Herzler J, Fikri M, Schulz C. High-pressure shock-tube study of the ignition and product formation of fuel-rich dimethoxymethane (DMM)/air and CH_4/DMM/air mixtures. Combust Flame 2020;216:293–9.
[10] Lindner F, Braun-Unkhoff M, Naumann C, Methling T, Köhler M, Riedel U. An experimental speciation study of DME, OME_1, and OME_2 in a single-pulse shock tube at high pressures. Combust Flame 2025;272:113883.
[11] Gaiser N, Bierkandt T, Oßwald P, Zinsmeister J, Kathrotia T, Shaqiri S, et al. Oxidation of oxymethylene ether (OME_{0-5}): an experimental systematic study by mass spectrometry and photoelectron photoion coincidence spectroscopy. Fuel 2022;313:122650.
[12] Gaiser N, Bierkandt T, Oßwald P, Zinsmeister J, Hemberger P, Shaqiri S, et al. Oxidation of linear and branched ethers: a comparative flow reactor study of OME_2 and trimethoxymethane. Proc Combust Inst 2023;39:685–93.
[13] Gaiser N, Zhang H, Bierkandt T, Schmitt S, Zinsmeister J, Kathrotia T, et al. Investigation of the combustion chemistry in laminar, low-pressure oxymethylene ether flames (OME_{0-4}). Combust Flame 2022;243:112060.
[14] De Ras K, Kusenberg M, Vanhove G, Fenard Y, Eschenbacher A, Varghese RJ, et al. A detailed experimental and kinetic modeling study on pyrolysis and oxidation of oxymethylene ether-2 (OME-2). Combust Flame 2022;238:111914.
[15] De Ras K, Kusenberg M, Thybaut JW, Van Geem KM. Unraveling the carbene chemistry of oxymethylene ethers: Experimental investigation and kinetic modeling of the high-temperature pyrolysis of OME-2. Proc Combust Inst 2023;39:125–33.
[16] De Ras K, Panaget T, Fenard Y, Aerssens J, Pillier L, Thybaut JW, et al. An experimental and kinetic modeling study on the low-temperature oxidation of oxymethylene ether-2 (OME-2) by means of stabilized cool flames. Combust Flame 2023;253:112792.
[17] De Ras K, Herbinet O, Battin-Leclerc F, Fenard Y, Tran L-S, Vanhove G, et al. Van Geem, a fundamental investigation of the pyrolysis chemistry of Oxymethylene Ethers. Part I: Quantum chemical calculations and kinetic model development. Combust Flame 2025;275:114121.
[18] De Ras K, Herbinet O, Battin-Leclerc F, Eschenbacher A, Kusenberg M, Varghese RJ, et al. Van Geem, a fundamental investigation of the pyrolysis chemistry of oxymethylene ethers. Part II: Experiments and comprehensive model analysis. Combust Flame 2025;275:114122.
[19] Wang H, Yao Z, Zhong X, Zuo Q, Zheng Z, Chen Y, et al. Experimental and kinetic modeling studies on low-temperature oxidation of polyoxymethylene dimethyl ether (DMM_{1-3}) in a jet-stirred reactor. Combust Flame 2022;245:112332.
[20] Zhong X, Wang H, Zuo Q, Zheng Z, Wang J, Yin W, et al. Experimental and kinetic modeling studies of polyoxymethylene dimethyl ether (PODE) pyrolysis in jet stirred reactor. J Anal Appl Pyrol 2021;159:105332.
[21] Qiu Z, Zhong A, Huang Z, Han D. An experimental and modeling study on polyoxymethylene dimethyl ether 3 ($PODE_3$) oxidation in a jet stirred reactor. Fundam Res 2022;2:738–47.
[22] Sun W, Wang G, Li S, Zhang R, Yang B, Yang J, et al. Speciation and the laminar burning velocities of poly(oxymethylene) dimethyl ether 3 ($POMDME_3$) flames: an experimental and modeling study. Proc Combust Inst 2017;36:1269–78.
[23] Suzuki S, Ishii Y, Katsumi T, Kinoshita K, Sakaida S, Konno M, et al. Formation of polycyclic aromatic hydrocarbons in fuel-rich oxidation of toluene, toluene/dimethyl ether blend, and toluene/oxymethylene ether-3 blend. Energy Fuels 2024;38:16911–23.
[24] Vermeire FH, Carstensen H-H, Herbinet O, Battin-Leclerc F, Marin GB, Van Geem KM. Experimental and modeling study of the pyrolysis and combustion of dimethoxymethane. Combust Flame 2018;190:270–83.
[25] Peukert S, Sela P, Nativel D, Herzler J, Fikri M, Schulz C. Direct measurement of high-temperature rate constants of the thermal decomposition of dimethoxymethane, a shock tube and modeling study. Chem A Eur J 2018;122:7559–71.
[26] Cai L, Jacobs S, Langer R, vom Lehn F, Heufer KA, Pitsch H. Auto-ignition of oxymethylene ethers (OME_n, n = 2–4) as promising synthetic e-fuels from renewable electricity: shock tube experiments and automatic mechanism generation. Fuel 2020;264:116711.
[27] He T, Wang Z, You X, Liu H, Wang Y, Li X, et al. A chemical kinetic mechanism for the low- and intermediate-temperature combustion of polyoxymethylene dimethyl ether 3 [PODE3]. Fuel 2018;212:223–35.
[28] Shrestha KP, Eckart S, Drost S, Fritsche C, Schießl R, Seidel L, et al. A comprehensive kinetic modeling of oxymethylene ethers (OME_n, n=1–3) oxidation - laminar flame speed and ignition delay time measurements. Combust Flame 2022;246:112426.
[29] Dinelli T, Pegurri A, Bertolino A, Parente A, Faravelli T, Mehl M, et al. A data-driven, lumped kinetic modeling of OME_{2-5} pyrolysis and oxidation. Proc Combust Inst 2024;40:105547.
[30] Kathrotia T, Bierkandt T, Gaiser N, Richter S, Lindner F, Jacobs S, et al. Combustion kinetics of alternative fuels, Part-IV: Extending reaction mechanism "DLR Concise" to include oxygenates for transportation fuels. Combust Flame 2024;271:113841.
[31] Jacobs S, Döntgen M, Alquaity ABS, Kopp WA, Kröger LC, Burke U, et al. Detailed kinetic modeling of dimethoxymethane. Part II: Experimental and theoretical study of the kinetics and reaction mechanism. Combust Flame 2019;205:522–33.
[32] Shrestha KP, Eckart S, Elbaz AM, Giri BR, Fritsche C, Seidel L, et al. A comprehensive kinetic model for dimethyl ether and dimethoxymethane oxidation and NO_x interaction utilizing experimental laminar flame speed measurements at elevated pressure and temperature. Combust Flame 2020;218:57–74.
[33] Kathrotia T, Oßwald P, Naumann C, Richter S, Köhler M. Combustion kinetics of alternative jet fuels, Part-II: Reaction model for fuel surrogate. Fuel 2021;302:120736.
[34] Schmitt S, Gaiser N, Zhang H, Stagni A, Bachmann J, Oßwald P, et al. Combining mass spectrometry, i^2PEPICO, and FTIR spectroscopy: Comprehensive speciation in DMM/NO oxidation. Proc Combust Inst 2024;40:105365.
[35] Bierkandt T, Gaiser N, Bachmann J, Oßwald P, Köhler M. Terpene speciation: Analytical insights into the oxidation and pyrolysis of limonene and 1,8-cineole via molecular-beam mass spectrometry. Combust Flame 2025;272:113854.
[36] Oßwald P, Köhler M. An atmospheric pressure high-temperature laminar flow reactor for investigation of combustion and related gas phase reaction systems. Rev Sci Instrum 2015;86:105109.
[37] Werner F, Kathrotia T, Bierkandt T, Schmid J, Gaiser N, Bachmann J, et al. Oxidation of MTBE and ETBE at atmospheric and elevated pressure. Proc Combust Inst 2025;41:105863.

[38] Taylor GI. Dispersion of soluble matter in solvent flowing slowly through a tube. Proc R Soc Lond A 1953;219:186–203.
[39] Aris R. On the dispersion of a solute in a fluid flowing through a tube. Proc R Soc Lond A 1956;235:67–77.
[40] Rasmussen CL, Hansen J, Marshall P, Glarborg P. Experimental measurements and kinetic modeling of $CO/H_2/O_2/NO_x$ conversion at high pressure. Int J Chem Kinet 2008;40:454–80.
[41] Hoener M, Kaczmarek D, Bierkandt T, Bodi A, Hemberger P, Kasper T. A pressurized flow reactor combustion experiment interfaced with synchrotron double imaging photoelectron photoion coincidence spectroscopy. Rev Sci Instrum 2020;91:045115.
[42] Lazzara CP, Biordi JC, Papp JF. Concentration profiles for radical species in a methane-oxygen-argon flame. Combust Flame 1973;21:371–82.
[43] D.G. Goodwin, R.L. Speth, H.K. Moffat, B.W. Weber, Cantera: An object-oriented software toolkit for chemical kinetics, thermodynamics, and transport processes, http://www.cantera.org, Version 2.5.1, 2021.
[44] Chemical Workbench, Kintech Lab, Version 4.1.19528, 2017.
[45] Pegurri A, Dinelli T, Pratali Maffei L, Faravelli T, Stagni A. Coupling chemical lumping to data-driven optimization for the kinetic modeling of dimethoxymethane (DMM) combustion. Combust Flame 2024;260:113202.
[46] Yu T, Wu X, Zhou X, Bodi A, Hemberger P. Hydrogen migration as a potential driving force in the thermal decomposition of dimethoxymethane: New insights from pyrolysis imaging photoelectron photoion coincidence spectroscopy and computations. Combust Flame 2020;222:123–32.